Structural, electronic and energetic properties of giant icosahedral fullerenes up to C6000. Insights from an *ab initio* hybrid DFT study

Y. Noël,[1] M. De La Pierre,[2] C.M. Zicovich-Wilson,[3] R. Orlando,[2] and R. Dovesi[2]

[1]*Institut des Sciences de la Terre de Paris (UMR 7193 UPMC-CNRS), UPMC, Sorbonne Universités, Paris, France*

[2]*Dipartimento di Chimica, Università di Torino and NIS, Nanostructured Interfaces and Surfaces, Centre of Excellence, Via P. Giuria 7, 10125 Torino, Italy*

[3]*Facultad de Ciencias, Universidad Autónoma del Estado de Morelos, Av. Universidad, 1001, Col. Chamilpa, 62209 Cuernavaca (Morelos), Mexico*

(Dated: May 14, 2014)

Abstract

Properties of the (n, n) icosahedral family of carbon fullerenes up to $n = 10$ (6000 atoms) have been investigated through *ab initio* quantum-mechanical simulation by using a gaussian type basis set of double zeta quality with polarization functions (84000 atomic orbitals for the largest case), the hybrid B3LYP functional and the CRYSTAL14 code featuring generalization of symmetry treatment. The geometry of giant fullerenes shows hybrid features, between a polyhedron and a sphere; as n increases, it approaches to the former. Hexagon rings at face centres take a planar, graphene-like configuration; the 12 pentagon rings at vertices impose however a severe structural constraint to which hexagon rings at the edges must adapt smoothly, adopting a bent (rather than sharp) transversal profile and an inward longitudinal curvature. HOMO and LUMO electronic levels, as well as the band gap, are well described using power laws. The gap is predicted to become zero for $n \geq 34$ (69360 atoms). The atomic excess energy with respect to the ideal graphene sheet goes to zero following a $\log(N_{at})/N_{at}$ law, which is well described through the continuum elastic theory applied to graphene; limits for the adopted model are briefly outlined. Compared to larger fullerenes of the series, C60 shows unique features with respect to all the considered properties; C240 presents minor structural and energetic peculiarities, too.

Keywords: (n,n) fullerenes, energy vs graphene, geometry, band gap, all electron Gaussian type basis set, hybrid B3LYP functional, CRYSTAL code

Corresponding authors: yves.noel@upmc.fr (method) ; marco.delapierre@unito.it (results).

I. INTRODUCTION

Since the discovery of C60 in 1985[1], fullerenes have attracted major scientific interest in many respects. In particular, surface functionalization[2] and molecule trapping inside the cage[3] are opening the way to a wide range of applications for this class of materials, including use in catalysis, photovoltaics, photodetection[4–6]. Recently, fullerenes have been identified in deep space[7], and multi-walled fullerenes have been proposed as possible sources of cosmic spectroscopic features as well as intermediates to the formation of inter-stellar nanodiamonds[8,9].

In 1980 spheroidal carbon particles were observed[10], that were later recognized to be giant fullerene structures in the form of multi-walled fullerenes, showing either spherical or polyhedral shapes[11,12]. This finding raised the interest in the electronic structure calculations of these systems, in order to understand their structure as well as their relative stability compared to other carbon nanoforms[13–21]. However, this pathway turned out to be extremely challenging, as the large number of atoms implied extremely high computational costs.

The first *ab initio* local density functional studies on C240 date back to the early 90s[13,14]; specific expedients had to be adopted to make the calculations feasible, such as geometry optimization with empirical potentials[13] or divide-and-conquer algorithms that by-pass the Kohn-Sham equations[14]. In 1995, an *ab initio* Hartree-Fock optimization of C240 and C540 was performed, by adopting a minimal STO-3G basis set[17]. In the same years, larger fullerenes, up to 8640 atoms[19], could be investigated by using low levels of theory, such as MNDO[18], Hückel[15,16] and Tight Binding[19]; the study by Xu and Scuseria[19] was first to evaluate the relative stability of fullerenes compared to graphene. *Ab initio* studies with more than 540 atoms and up to 2160 are very recent (2006)[20], and have not gone beyond the level of local density approximation.

Among the above mentioned studies, only four of them report about the use of icosahedral symmetry to reduce the cost of the calculation[13,15,17,20] and only three of them adopt a publicly available code[17,18,21]. More notably, while discussing yet relevant geometrical aspects such as the sphere *vs* polyhedron shape, none of these investigations present a detailed

analysis of the structure of fullerenes (relaxation from the as-folded icosahedron structure; trends with large n). Finally, only in recent cases the relative stability compared to the graphene sheet was investigated[19–21] at the *ab initio* level, the limiting factors being either the low level of adopted theory[19] or the small number of investigated members[20,21].

The first aim of the present study is to illustrate the scheme adopted for the automatic construction of fullerenes within the public quantum-mechanical periodic code CRYSTAL14[22,23]. Icosahedral, octahedral and tetrahedral fullerenes can be built starting from a two-dimensional sheet, with no need for importing data generated by other codes. Corresponding point symmetries are exploited all along the electronic structure calculation. While there exist some publicly distributed utilities for the generation of fullerene structures, e.g. *Fullerene*[24] and *CaGe*[25], the only other public code with exploitation of icosahedral symmetry seems to be the molecular program TURBOMOLE[26].

The second aim is to present the results of an accurate, homogeneous and detailed computational study of the structure, electronics and energetics of icosahedral carbon fullerenes with up to 6000 atoms; the graphene monosheet, treated at the same level of theory (exchange-correlation density functional, basis set) is taken as a reference, and carbon nanotubes with up to 1360 atoms are presented for cross-comparisons. Total energy calculations and geometry optimizations are carried out by using a level of theory higher than in any other previous study, namely the hybrid Hartree-Fock / Density Functional B3LYP Hamiltonian[27–29], and an all electron Gaussian-type basis set. To the authors' knowledge, the molecules investigated in the present study are the largest ever simulated by means of density functional electronic structure methods.

This paper is structured as follows. Section II presents the computational framework of the calculations and illustrates the scheme for automatic generation of fullerenes. Section III describes the analysis of structure, electronic levels and energy of giant icosahedral fullerenes. Section IV summarizes the main results.

Additional information is available as Supplementary Material; Figures and Tables in this Section are labelled with the "S" prefix.

II. METHOD

A. Computational Details

The CRYSTAL14 periodic *ab initio* code[22,23] was used, featuring state-of-the-art full exploitation of symmetry. Maximum advantage is taken of the highly symmetric icosahedral point group (I_h, 120 operators) at all stages of the electronic structure calculation, direct transformations are performed between the bases of Atomic Orbitals (AOs) and Symmetry Adapted Molecular Orbitals (SAMOs), and allocation of full matrices in the basis of AOs is always avoided. Performance in terms of CPU time and memory allocations is discussed in detail in Refs. 30–32. For the largest case here considered, a (10,10) fullerene, the number of AOs is $N = 84000$, so that the size of a single $N \times N$ matrix depasses 50 GBytes; however, in the SAMO basis the largest dimension decreases to 3530, so that only 100 MBytes are required for the allocation of matrices to be diagonalized. A complete SCF energy calculation for (10,10) runs on a single processor with 2 GB RAM in about 24 hours.

Calculations were performed with the B3LYP hybrid functional[27–29], which has recently been applied to the study of structural, vibrational and optical properties of semiconducting C and BN nanotubes[33–37] and graphene-derived sheets[38]. Carbon atoms were described using a 6-31G(d)[39] Gaussian-type basis set, consisting of 14 AOs per atom. The same basis set has recently been adopted for the study of other carbon compounds with similar chemistry, such as nanotubes[34] and polyacetylene[40,41].

The level of accuracy in evaluating the bielectronic Coulomb and Hartree-Fock exchange series is controlled by five parameters T_i $(i = 1, ...5)$[22]. T_1 and T_2 refer to the Coulomb series, T_3, T_4 and T_5 to the exchange ones: integrals are disregarded when the *overlap* between the corresponding basis functions is below 10^{-T_i}. More details on these truncation criteria can be found in Refs.[22,40]. In this study the values of 8, 8, 8, 8, 20 were chosen. The threshold on the SCF energy for geometry optimization was set to 10^{-8} Ha.

The DFT exchange-correlation contribution is evaluated by numerical integration over the unit cell volume. In CRYSTAL, radial and angular points of the grid are generated through Gauss-Legendre radial quadrature and Lebedev two-dimensional angular point distributions. A (75,974)p grid was used, corresponding to a pruned grid with 75 radial and 974 angular points (XLGRID keyword in the CRYSTAL manual[22]). Accuracy of this grid can be

estimated from the error on the integrated electronic charge density in the unit cell, that amounts to less than 0.0003% for C_{60} (it gets smaller in the case of larger fullerenes).
Structures were optimized by using the total energy analytical energy gradients with respect to atomic coordinates and unit cell parameters[42–44], within a quasi-Newtonian scheme combined with the BFGS algorithm for Hessian updating[45–48]. Convergence was checked on both gradient components and nuclear displacements, for which default values[22] were chosen.
Reference calculations for graphene, corannulene and nanotubes were performed with the same parameters as for fullerenes. For graphene the reciprocal space was sampled along the 2 lattice vectors according to a sublattice with shrinking factor[22] set to 56 according to Ref. 38, corresponding to 290 independent $\vec{k}$ vectors in the irreducible part of the Brillouin zone. For nanotubes, sampling of the reciprocal space along the unique lattice vector was performed using a shrinking factor set to 40, corresponding to 21 independent $\vec{k}$ vectors[34].
Manipulation and visualization of structures were performed with the Jmol 3D engine[49,50]. Molecular drawings were rendered with the Inkscape program[51] using input files prepared with Jmol. Data analysis was performed using the LibreOffice suite[52] and the Octave environment[53]. Graphs were realized with the Gnuplot utility[54].

B. Construction of fullerenes from a graphene monolayer

In the CRYSTAL14 code fullerenes are built automatically starting from any hexagonal sheet, by using the `FULLE` keyword (a typical geometry input block is shown in Figure S1 in the Supplementary Information). The first required information are two integers, n_1 and n_2, defining the components of the **R** vector in terms of the basis vectors $\vec{a}_1$ and $\vec{a}_2$ of the hexagonal unit cell (see Figure 1). The scheme allows for different types of polyhedra with diverse point groups to be constructed; these represent the third and second requested input information, respectively. The choice of the polyhedron constrains the point group: I and I_h (`I` and `IH` input options, respectively) are only compatible with icosahedron (`ICOSA` input option); T_h, O and O_h (`TH`, `O` and `OH`) with octahedron (`OCTA`); T and T_d (`T` and `TD`) with both tetrahedron (`TETRA`) and octahedron.
The **R** vector is the side of the equilateral triangle (in pink in Figure 1), that constitutes a face of the polyhedron on which the fullerene is built. Only the three atoms (the example

refers to the (2,2) fullerene) in the irreducible portion (in dark pink) are required for the construction of the fullerene, as the code uses symmetry. The new cartesian reference for the fullerene is set so that the origin O coincides with the geometric center of the polyhedron, the x axis is parallel to the $\mathbf{R}$ vector and the z axis is normal to the first-built triangular face. The radii of the spheres inscribed and circumscribed to the polyhedron correspond to the distances of the origin O from the triangle center and vertices, respectively. The symmetry point group is built so that all rotation axes are concurrent in the origin O. All symmetry operators are then applied to all irreducible atoms, generating the complete set of atoms. In the case of icosahedral, octahedral and tetrahedral fullerenes, 20, 8 and 4 triangular faces are generated, respectively.

Figures S2 and S3 in the Supplementary Information provide additional details on the procedure. Further resources on the construction of fullerenes from a sheet, including animations and more pictorial representations, can be found in the new CRYSTAL Web Tutorial on fullerenes at `www.crystal.unito.it` → Tutorials → Fullerene systems.

C. General properties of icosahedral fullerenes

The (n, n) icosahedral fullerenes investigated in this study have point group symmetry I_h, characterized by the identity operator plus 12 C_5, 12 C_5^2, 20 C_3, 15 C_2 axes, i (inversion), 12 S_{10}, 12 S_{10}^3, 20 S_6 axes and 15 σ (mirror planes), leading to a total of 120 symmetry operators. For this series, it holds that $n_1 = n_2 = n$, where n_1 and n_2 have been defined in Section II B above, and n ranges from 1 to 10.

For these fullerenes, simple functions of n can be derived that give the values for some relevant quantities reported in Table I. In particular:

- Number of irreducible atoms n_{at}:

$$n_{at} = \frac{n(n+1)}{2} \tag{1}$$

- Total number of atoms N_{at}:

$$N_{at} = 60 \cdot n^2 \tag{2}$$

  As each atom has 3 bonds shared with other atoms, i.e. accounting for 3/2 bonds, the number of bonds is $N_{bond} = 3/2 \cdot N_{at} = 90 \cdot n^2$.

- Number of hexagons N_{hex}:

$$N_{hex} = 30 \cdot n^2 - 10 \tag{3}$$

  Note that the number of pentagons N_{pent} is independent of n and always equal to 12.

- Number of degrees of freedom N_{DOF}:

$$N_{DOF} = \frac{n(3n+1)}{2} \tag{4}$$

  This quantity indicates how many variables the energy gradient is a function of, and is relevant in the algorithms for geometry optimization. For large n, N_{DOF} tends to $3 \cdot n_{at}$ (for comparison, it equals $3 \cdot (N_{at} - 2)$ if symmetry is not exploited).

The above formulas permit to compute also the ratio $\rho_{at} = N_{at}/n_{at}$:

$$\rho_{at} = \frac{N_{at}}{n_{at}} = 120\frac{n}{n+1} \tag{5}$$

Atoms in fullerenes lie either on edges or on faces, with multiplicities (i.e. number of symmetry related atoms) of 60 or 120, respectively. For $n = 1$, ρ_{at} is equal to 60 (all atoms on edges). With increasing n, the value of ρ_{at} increases and tends to 120 (atoms on faces much more than atoms on edges); for $n = 10$ it is about 109. This ratio approximates the saving factor in the SCF energy calculation due to symmetry exploitation[31], as various steps of the calculation can be performed on the subset of n_{at} irreducible atoms, rather than on the full set of N_{at} atoms.

III. RESULTS

A. Structure: radial distances

Atomic radial distances for the fullerene cages, as obtained from simulation, are given in Table II and represented graphically in Figure 2. In the following, we will indicate as "radius" the distance of the atoms from the cage centre.

The (1,1) fullerene is the only case where all atoms have the same radius, 3.544 Å (they lie on a sphere). In all other cases both the minimum and maximum radii, r_{min} and r_{max} (see Table II), grow linearly with n, ranging from 6.940 and 7.332 Å for (2,2), to 33.608 and 39.660 Å

for (10,10); they correspond to atoms lying on face centres and vertices, respectively. The average radius $< r >$ (crosses in Figure 2) obeys the linear relation:

$$< r >= (3.489 \cdot n + 0.072) \text{ Å } = [3.489 \cdot (n + 0.021)] \text{ Å} \quad (6)$$

As the intercept of this line is as small as 0.072 Å, its slope turns out to be quite close to the radius of the smallest fullerene ($n = 1$, $< r >= 3.544$ Å), the deviation being 1.5%. Average radii for large fullerenes could therefore be extrapolated with good accuracy using only the value for (1,1). The difference between the maximum and minimum radii, Δr, obviously obeys a linear relation, too (diamonds in Figure 2); it is equal to 0 Å for the (1,1) fullerene, increases to 0.392 Å for (2,2), and reaches 6.052 Å for (10,10). The ratio $\rho_r = r_{max}/r_{min}$ increases monotonically from 1 to 1.180.

We can compare r_{min} and r_{max} with the values for two ideal situations: a sphere with radius $< r >$, and an icosahedron as obtained from the construction described in Section II B; the latter is characterized by a minimum radial distance $r_{p,min}$ at face centres and a maximum radial distance $r_{p,max}$ at vertices. All these quantities are shown in Figure 2. The corresponding differences can be defined (see also Figure S4 in the Supplementary Information): $\delta_{<r>,min} = r_{min} - < r >$ and $\delta_{<r>,max} = r_{max} - < r >$ for the sphere, and $\delta_{p,min} = r_{min} - r_{p,min}$ and $\delta_{p,max} = r_{max} - r_{p,max}$ for the polyhedron. In the case of (1,1) all differences are 0, as this fullerene is a perfect icosahedron with all atoms lying on a sphere. Radii of the (2,2) fullerene are as close to the sphere as to the polyhedron ones (Figure 2 and Figure S4). From $n = 3$ on, fullerene radii are always closer to the polyhedron rather than to the sphere case. In comparison with the average sphere, differences can be as large as 4.69 Å in modulus in the case of (10,10), indicating a significant divergence of the series of fullerenes from sphericity. Looking at the polyhedron case, $\delta_{p,max}$ has an almost constant value, $\approx$ -0.21 Å, suggesting that the fullerene vertices have almost the same radial distance as in the corresponding icosahedra. On the other hand, the difference $\delta_{p,min}$ increases linearly with n, from 0.40 Å in (3,3) to 1.30 Å in (10,10). This indicates that the fullerene faces have a slightly but increasingly larger radius compared to the icosahedron, and gives evidence for a modest yet not negligible deviation from the polyhedral shape.

B. Structure: curvature profiles

Figure 3 shows the structure of the (5,5) fullerene, taken as a reference in this discussion; a path has been drawn along the cage, that includes the three types of rotation axes (C_2, C_5 and C_3 in green, yellow and pink, respectively). The green portion of the path coincides with an edge of the triangular face, the red one is perpendicular to it. Figure 4 shows a section of this path for all the (n, n) fullerenes studied here. Angles α, β and γ between rotation axes have fixed values imposed by the icosahedral point group symmetry (31.7°, 37.4° and 20.9°, respectively). Let us analyze the components of these angular values along the path (right side of Figure 4); we will start our discussion from $n = 2$, as for (1,1) angles are constrained to α, β and γ values.

Pentagons at fullerene vertices (in yellow in Figure 4) are the regions with largest component angles all along the series. Indeed, the largest contributions to α and β are concentrated within the first two angles close to the C_5 axis along the green and red paths, respectively. Values for the first-closest angles are 25.9° and 26.6° for $n = 2$, and 27.8° and 28.2° for $n = 3$; for subsequent fullerenes, they are very similar to these latter values (reaching 28.2° and 28.6° for $n = 10$). Note that (2,2) shows the smallest values for these angles, i.e. its structure has the smallest curvature around pentagons. As a reference, corannulene $C_{20}H_{10}$ can be considered as the prototype for a single, "independent", mechanically unconstrained pentagonal vertex; it is made up of a pentagon ring surrounded by five hexagon rings saturated with hydrogens. In this molecule, angles close to the pentagon measure 22.4° and 21.7°, respectively; (2,2) is therefore the fullerene whose curvature at vertices comes closest to this prototypal case. The second-closest angle along the green path (edge) is 5.8° for $n = 2$, 4.7° for $n = 3$; from $n = 4$ on it does not change much, going from 5.3° to 5.6° ($n = 10$). The second-closest angle along the red path (face) is 10.7° for $n = 2$, due to proximity with the C_3 axis; it is converged for larger n, going from 5.1° ($n = 3$) to 5.2° ($n = 10$).

Fullerene edges (green paths in Figure 4) show a nearly planar section from (3,3) on; except for an angle of 1.5° for $n = 4$, all angles are smaller than 1.1°. Notably these small angles are negative in sign, implying that edges have a slight inward curvature, which increases with n. Note that also edge angles close to the C_2 axis are small.

The red path goes along a fullerene face; two sub-regions can be identified, namely between

C_5 and C_3 axes (from vertex to face centre), and between C_3 and C_2 axes (from face centre to edge centre). In the former case, the profile is practically planar from $n = 4$ on, when an angle smaller than 1° first appears. For larger n and with the exception of angles close to either C_5 or C_3 axes, the largest angle in this sub-region is 1.1°. In this case, angles are generally positive in sign, indicating a very slight outward curvature.

The second sub-region of the red path, from face centre to edge centre, has a peculiarity: it is the only case where non-negligible components of the macroscopic angle (γ) are distributed all along the path, rather than being concentrated close to the axes, so that even for $n = 10$ the smallest absolute angular value is as large as 2.5°. The unique angle for $n = 2$ coincides with γ, 20.9°; for $n = 3$ values are 11.8° and 18.1°, for $n = 4$, their value is 8.2° and 12.7°. The first fullerene with no angles larger than 10° is $n = 6$; finally, for $n = 10$, they are 2.5°, 3.5°, 4.4°, 5.1° and 5.4°. Note that angular values decrease from C_2 (transversal edge angles) to C_3 (face centre angles). Relatively large values are found also for the first angle just past the C_3 axis (10.7° for $n = 2$, 4.0° for $n = 3$, until 1.7° for $n = 10$); these angles prosecute the decreasing trend which has just been pointed out. The peculiarity of this sub-region indicates the tendency for edges to have a smooth transversal (outward) curvature penetrating into the fullerene faces; this configuration is preferred to sharp-angled, polyhedron-like edges.

As an overall trend, faces grow plane-wise in the centre and towards vertices, as in polyhedra. On the other hand, edges with smooth, curved transversal profiles are preferred to sharp edges, unlike in polyhedra. For increasing n, face features dominate over edge ones, so that fullerenes resemble polyhedra rather than spheres (see also Section III A above).

C. Structure: atomic displacements compared to ideal polyhedra

The left side of Figure 4 compares the fullerene profiles with those of ideal graphene-like triangular faces. While the inward bending of the edges has already been commented, the other remarkable aspect is the raising of the faces (compare red and black, straight, paths); this is a consequence of the outward curvature observed above along the red path. Real and polyhedral, "graphene-faced", fullerenes are compared in a more quantitative manner in Figure 5, where the corresponding atomic displacements are rendered through a color scale. The largest differences (red in the scale) are found for face centres, which show a rigid

raising along the out-of-face coordinate of 0.5, 0.9 and 1.3 Å in the cases of $n = 4$, 7 and 10, respectively. As just pointed out above, this raising is related to the outward curvature along the red path, which produces an increasing displacement going from edges and vertices (blue in the scale) to the face centres. If we consider only the "in-face" components of the relative displacements (Figure S5 in the Supplementary Information), regions with non-zero values are identified along the fullerene edges. Displacements are far smaller compared to the raising of face centres, their maximum value being about 0.1 Å in the case of $n = 10$. These displacements are responsible for the transversal smoothing of the edges, which has been discussed in Section III B.

D. Structure: bond lengths

The distribution of C-C bond lengths along the series is represented in Figure 6. The most abundant length value is 1.452 Å for $n = 1$ and 1.446 Å for $n = 2$; from $n = 3$ on, it is always comprised between 1.420 and 1.426 Å, i.e. very close to the C-C bond length in graphene, 1.422 Å. The minimum value is 1.392 Å for $n = 1$; it decreases to 1.384 Å for $n = 2$, and then increases monotonically until 1.389 Å ($n = 10$); this value always corresponds to bonds with one atom belonging to a pentagon (see below). The maximum value is 1.452, 1.446 and 1.438 Å for $n = 1$, 2 and 3, respectively; it remains nearly unaltered from $n = 4$ to $n = 10$, going from 1.433 to 1.432 Å. Starting from bonds with one atom belonging to a pentagon and moving far from the pentagon along the edge, the longest bond is the first one for $n =$ 1,2,5÷10; it is the third along the same path for $n =$ 3,4, instead.

The (1,1) fullerene has only two length values: 1.392 Å for hexagon-only bonds and 1.452 Å for pentagon-hexagon shared bonds. For all other fullerenes, bonds can be classified in three types. The first includes bonds in pentagons, whose unique value is 1.425, 1.421 and 1.421 Å for $n = 2$, 3 and 10, respectively; this value is always very close to the C-C bond length in graphene. The second includes bonds with one atom belonging to a pentagon, with a unique value of 1.384, 1.386 and 1.389 Å ($n = 2$, 3 and 10); this is always the shortest C-C distance in the structure. The third type includes all other C-C bonds (hexagons), with values ranging from 1.422 to 1.446 Å for $n = 2$, from 1.410 to 1.438 Å for $n = 3$, and from 1.416 to 1.432 Å for $n = 10$.

As a final remark on structural features, we note that in the previous literature[14,17–19,21] there

has been a long discussion concerning the either spherical or faceted shape of giant fullerenes, with a final general agreement on the latter hypothesis. The present study confirms this view, while enriching it in qualitative description and quantitative structural details. The most remarkable aspects concern the fullerene edges, with their longitudinal inward curvature and transversal smooth profile, and the first two fullerenes of the series, exhibiting unique characteristics in terms of radial distances, angular values and bond lengths.

E. Electronic levels

Diagrams of the electronic eigenvalues are shown in Figure 7; the x and y axes correspond to energy, in eV, and degeneracy, respectively. HOMO and LUMO energies always have a degeneracy of 5 and 3, respectively; this qualitative finding agrees with previous Hückel[15,16], HF[17] and LDA[13] studies. Using Eq. (2), it turns out that a (n, n) fullerene has $180 \cdot n^2$ occupied Molecular Orbitals. Symmetry analysis shows that there are $48 \cdot n^2$ degenerate occupied energy levels; two thirds of them, i.e. $32 \cdot n^2$, correspond to valence levels.
Let us now concentrate on the behavior of the HOMO/LUMO levels and of the band gap with increasing n; data are reported in Table II and plotted in Figure 8 (note that the x axis reports $1/n$). Values of E_{HOMO} and E_{LUMO} as a function of n are very well described by means of power laws, which imply log-log linear behaviors, provided that data for (1,1) are excluded; we will come back to this aspect later. Best-fits with three parameters provide the following expressions:

$$E_{HOMO} = \left(-3.45 - 2.41 \cdot n^{-0.53}\right)\ eV \tag{7}$$

$$E_{LUMO} = \left(-3.85 + 1.33 \cdot n^{-1.14}\right)\ eV \tag{8}$$

Note that E_{LUMO} has a dependence quite close to n^{-1}, whereas for E_{HOMO} the exponent for n is close to $-\frac{1}{2}$ (inverse square root).
The electronic band gap E_{gap} is as large as 2.711 eV for (1,1); it equals 1.888 eV for (2,2), and drops down to 0.420 eV at (10,10). A quite satisfactory fit, again excluding (1,1), is obtained by combining the two previous ones ($E_{gap} = E_{LUMO} - E_{HOMO}$):

$$E_{gap} = \left(-0.40 + 1.33 \cdot n^{-1.14} + 2.41 \cdot n^{-0.53}\right)\ eV \tag{9}$$

For $n \geq 23$ the predicted gap is smaller than 0.1 eV; when $n \geq 34$, the band gap is expected to become zero. Similar power laws for the three quantities were proposed in Ref. 16; the

values of the fitting parameters are rather different, which is likely related to the rather different level of approximation adopted in that study (π electrons only, Hückel theory). Figure 8 shows that HOMO and LUMO levels of the smallest fullerene are higher and lower, respectively, than the fitted values, which in turn results in an electronic gap smaller than expected. A possible reason for this anomalous behavior is the occurrence of only one symmetry irreducible atom in (1,1), which forbids differentiation between atoms (and molecular orbitals) related to pentagon rings and those related to hexagon rings.

F. Stability compared to graphene

Table II reports the excess energy per atom ΔE_{at} of (n, n) fullerenes (in meV/atom), where the ideal, planar graphene sheet is taken as a reference. This quantity is as large as 412.7 meV/atom for (1,1), drops down to 154.8 and 91.0 meV/atom for (2,2) and (3,3), and reaches 13.4 meV/atom for (10,10). A convenient graphical representation is given in Figure 9; it involves the excess energy per molecule ΔE_{mol}, which equals $\Delta E_{at} \cdot N_{at}$, as a function of the logarithm of the number of atoms N_{at}. This view highlights the logarithmic behavior of the molecular excess energy, which implies that the atomic excess energy goes to zero like $\log(N_{at})/N_{at}$.

A simple model can be found in the literature[55–57] that permits to describe the observed behavior in the framework of elastic continuum theory of graphene. A quantity necessary for this description is the bending modulus (or flexural rigidity) D of graphene; it has the dimension of an energy and can be defined as the amount required to bend a graphene sheet having unit area into a cylindrical tube with unit curvature. In order to compute D, we shall consider carbon nanotubes, and note that their bending energy ΔE_{area} (irrespective of the rolling direction) has a linear dependence on the square of the tube curvature, $k^2 = 1/r^2$, the proportionality factor being equal to $D/2$[58,59]. We here consider a large set of $(n, 0)$ nanotubes with n ranging from 8 to 340 (Table S1 and Figure S6 in the Supplementary Information). If we took into account tubes with small radii (i.e. large curvatures), D would be overestimated by as much as 10%, as the corresponding bending energies deviate from the simple linear behavior (Figure S6). By disregarding smaller tubes and fitting the data for $n = 200 \div 340$, we find a well converged value $D = 1.61$ eV for the bending modulus of graphene. Previous *ab initio* studies give 1.49 eV (Ref. 60, LDA level, and Ref. 61, GGA)

and 1.52 eV (Ref. 62, LDA); differences with respect to the present result might be due to the adopted functionals. Calculations with various empirical force-fields yield even smaller values: 1.02 eV (Ref. 56), 0.86 and 1.09 eV (Ref. 57).

Now, let us turn back to the elastic continuum model for fullerenes. It describes an icosahedral fullerene as a superposition of 12 conical frusta, whose smaller bases are located at the icosahedron vertices. A single frustum can be obtained by taking a graphene sheet, cutting out a 60° wedge starting from an hexagon centre, and joining the cut edges together. The resulting fivefold ring represents a "disclination" in the ideal graphene sheet, and an expression for its elastic energy can be easily derived[56,57]; the final formula for the entire fullerene includes a factor of 12:

$$\Delta E_{mol} = 12E_5 + \frac{11\pi}{5} D \log \frac{N_{at}}{60} \tag{10}$$

here E_5 is related to the energy of a pentagonal disclination (carbon pentagon plus neighborhoods); most important, D is the bending modulus of graphene. Figure 9 clearly indicates that fullerenes from (3,3) on strictly follow the proposed logarithmic law.

A best-fit of energy data for fullerenes with $n = 3 \div 10$ gives well converged parameter values of 1.88 eV for the bending energy D and 1.74 eV for the disclination energy. The value for D is 17 % larger than the one obtained above from the set of nanotubes. The origin of this discrepancy lies on the approximations inherent to the elastic model at the basis of Eq. (10). The most relevant is the assumption of circular rotational symmetry of the disclination[55]; instead, the 12 conical frusta have joined bases, which gives each disclination a five-fold, rather than circular, rotational symmetry; this keeps the logarithmic behavior, but is expected to increase the coefficient[55,56]. We can give a measure of how much fullerenes from our *ab initio* simulations have disclinations deviating from the circular symmetry assumed in the elastic model: actually, this is related to the fullerene being rather dissimilar from a sphere, which is indeed what results from the discussion on structure in Sections III A and III B above. A second discrepancy from the model is that the centres of fullerene faces are not covered by the cones[57]; however, this affects excess energies to a little extent, as face centres are almost flat (thus similar to graphene). We could find only one study in the literature with a quantitative comparison between excess energies of carbon nanotubes and fullerenes[56]: the authors performed empirical force-field calculations, and found out a smaller discrepancy than ours, around 6 %. Another empirical study compares energies for the two types of structure without giving any quantitative detail on the observed discrepancies[57].

Finally, Figure 9 shows that energy for (1,1) is 4 eV/molecule larger than the value obtained with the logarithmic law; the reason for a larger excess energy of (1,1) compared to larger fullerenes is the same as for the observed anomalies in the electronic properties (see Section III E above): (1,1) has only one irreducible atom, and thus a reduced capability of relaxing in a proper way the structure of both hexagon and pentagon rings. The (2,2) fullerene is 1.7 eV/molecule more stable than expected from the logarithmic law, which is a discrepancy smaller than for (1,1); inclusion of its energy in the best-fit would result in small variations to the parameter values (they would be 1.93 and 1.62 eV). This additional stability compared to larger fullerenes (discussed, in other terms, in Ref. 63) reasonably arises from a smaller mechanical stress at vertex regions, which for the relatively small (2,2) fullerene still represent a relevant portion of the entire structure. Indeed, discussion in Section III B pointed out that (2,2) has the smallest curvature at vertices of the whole series, which makes it the closest fullerene to the corannulene molecule; the latter represents a mechanically unconstrained prototype for the pentagonal vertex region. Notably, force-field studies in the literature concerning the energetics of large fullerenes[56,57] present energies for (1,1) that are in remarkable agreement with the logarithmic law from the elastic theory; the present electronic structure calculations show that this is not the case. This suggests that the description of (1,1) fullerene using empirical force-fields may result in artifacts when comparing it to larger fullerenes.

IV. CONCLUSIONS

We have presented a comprehensive *ab initio* study on the properties of large carbon icosahedral fullerenes with up to 6000 atoms. Calculations were made feasible thanks to the implementation of fullerene symmetry and to the improved exploitation of symmetry along all steps of the electronic structure calculation in the public code CRYSTAL14.

A detailed and accurate analysis has been carried out on the structural properties of fullerenes. As shown in previous studies, large cages show features that are intermediate between those of a polyhedron and those of a sphere, yet closer to the former. Novel qualitative and quantitative details have been added to this picture; the most relevant ones concern (a) the shape of fullerene edges, with longitudinal inward curvature and transversal smooth (rather than sharp) profile, and (b) the unique characteristics exhibited by the first

two fullerenes of the series, C60 and C240.

The smallest fullerene of the series, C60, also shows unique electronic and energetic properties compared to larger structures: higher HOMO level, smaller band gap, higher excess energy. All these features are the consequence of C60 having only one symmetry irreducible atom, which does not permit its molecular orbitals to properly accomodate both pentagon and hexagon rings.

Excess energy of large fullerenes with respect to the graphene sheet excellently fits a logarithmic law that can be interpreted in terms of continuum elastic theory; this is shown here at the *ab initio* level for the first time. The observed discrepancy between the fitted value of the bending modulus of graphene and an independent value (inferred from accurate nanotube calculations) highlights the approximations in the elastic model adopted for fullerenes, in particular the assumption of circular rotational symmetry. C240 shows an excess energy slightly smaller than that expected from the logarithmic law; this additional stability is related to a smaller mechanical strain at the pentagonal vertex regions.

V. ACKNOWLEDGEMENTS

The authors acknowledge Compagnia di San Paolo for financial support (Progetti di Ricerca di Ateneo-Compagnia di San Paolo-2011-Linea 1A, progetto ORTO11RRT5). CZ acknowledges financial support from CONACyT through project CB-178853.

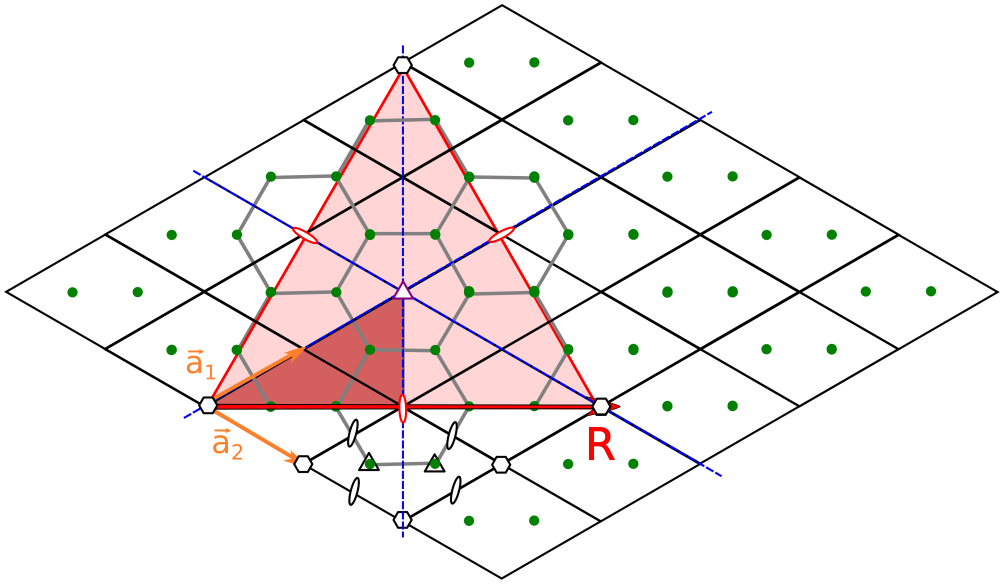

FIG. 1: Construction of the triangular face of the icosahedral (2,2) fullerene from graphene. $\mathbf{R} = 2 \cdot \vec{a}_1 + 2 \cdot \vec{a}_2$ is the side of face (see text). A $\gamma = 60°$ reference is assumed for the hexagonal two-dimensional lattice. The irreducible portion of the triangle is in dark pink; carbon atoms are shown in green; some symmetry operators are sketched: rotation axes and mirror planes (the latter in blue).

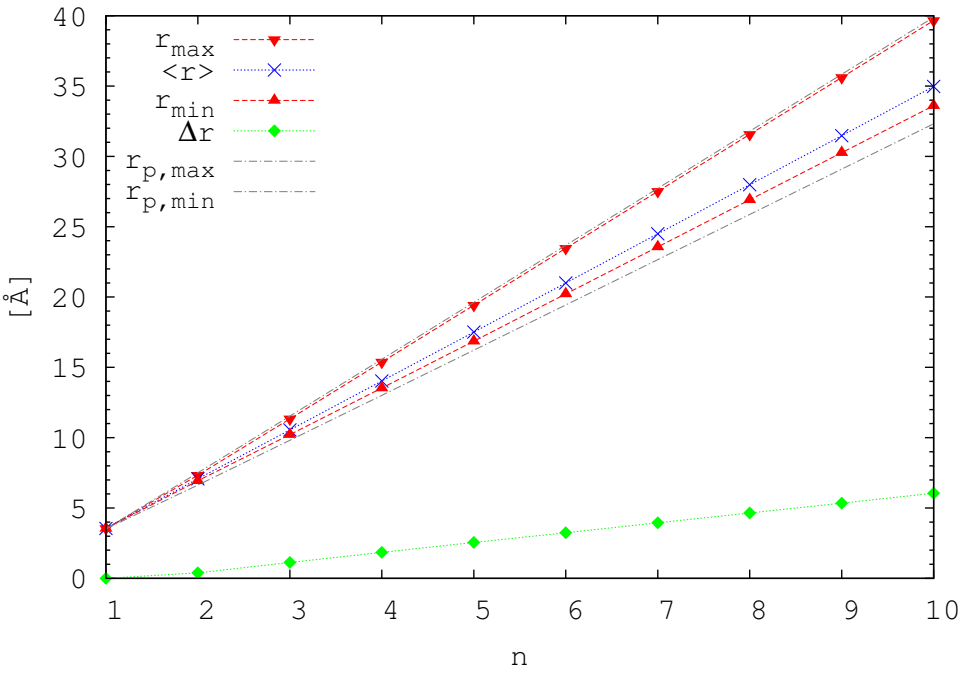

FIG. 2: Radii of the (n, n) fullerenes as a function of n (in Å). r_{min} and r_{max} are the minimum and maximum radial distances; Δr is their difference, $< r >$ is the average value over all atoms. Also the minimum ($r_{p,min}$) and maximum ($r_{p,max}$) distances in the as-built polyhedral fullerene are reported (the former is slightly lower than r_{min}; the latter nearly coincides with r_{max}).

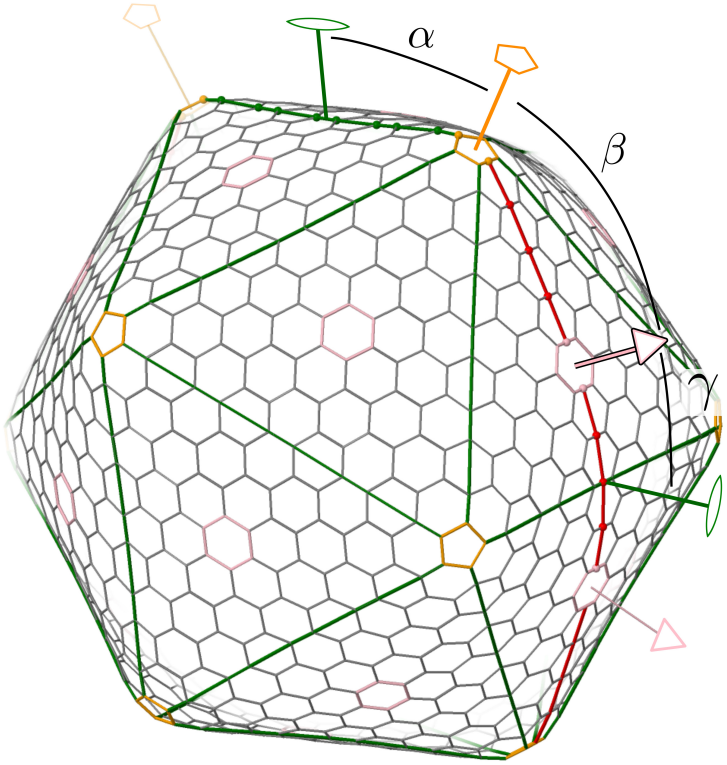

FIG. 3: The (5,5) fullerene structure; it is used as a reference for Figure 4. Pentagons and C_5 axes are in yellow; hexagons lying on the C_3 axes at the face centers are in pink, as well as the C_3 axes; fullerene edges and C_2 axes are in green. The angle between C_2 and C_5 axes is denoted as α; the angles between C_5 and C_3 axes and C_3 and C_2 axes are called β and γ, respectively. A path around the fullerene is defined; it is in red when it crosses a triangular face and in green when it follows an edge. Points along the path are emphasized, that are used in Figure 4; in the green portion of the path they correspond to carbon atoms; in the red portion they correspond to the middle of C-C bonds, instead.

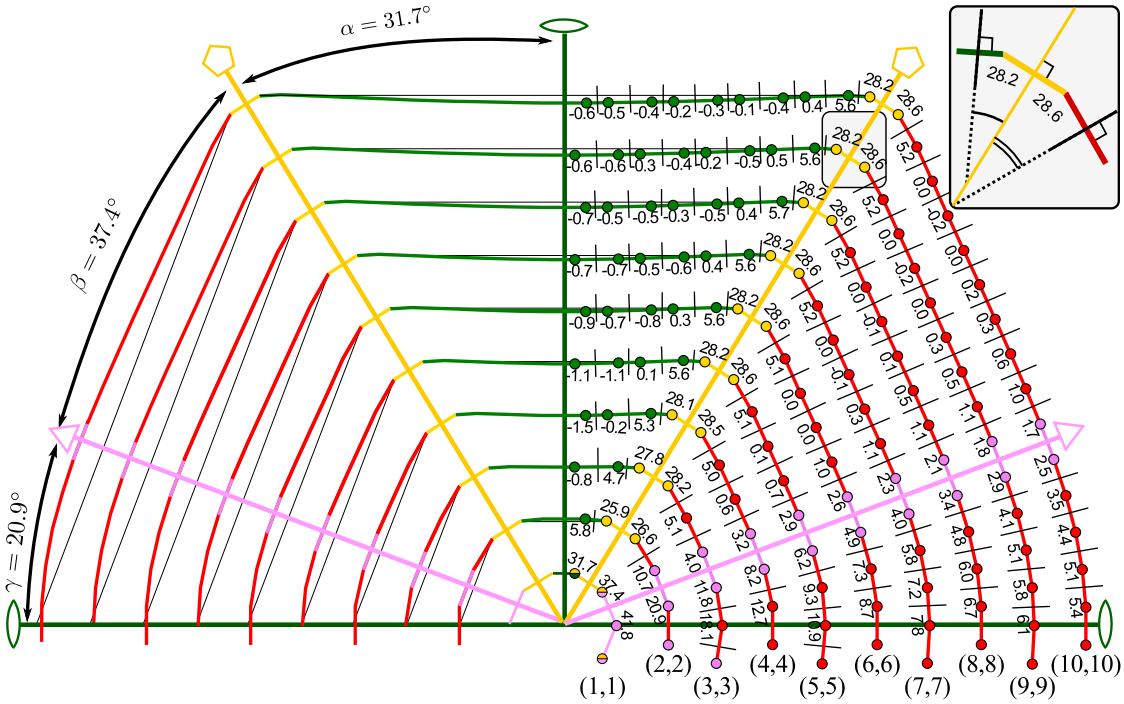

FIG. 4: Sections of (n, n) fullerenes, showing the paths described in Figure 3. All angles are in degrees. Two-, five- and three- fold rotation axes and the corresponding angles α, β and γ are constant along the whole fullerene series. Right side: components of α, β and γ along the path, corresponding to angles between the normals of two consecutive segments of the path (see inset on top). Left side: path profiles compared to the profiles of the ideal graphene sheet (black lines).

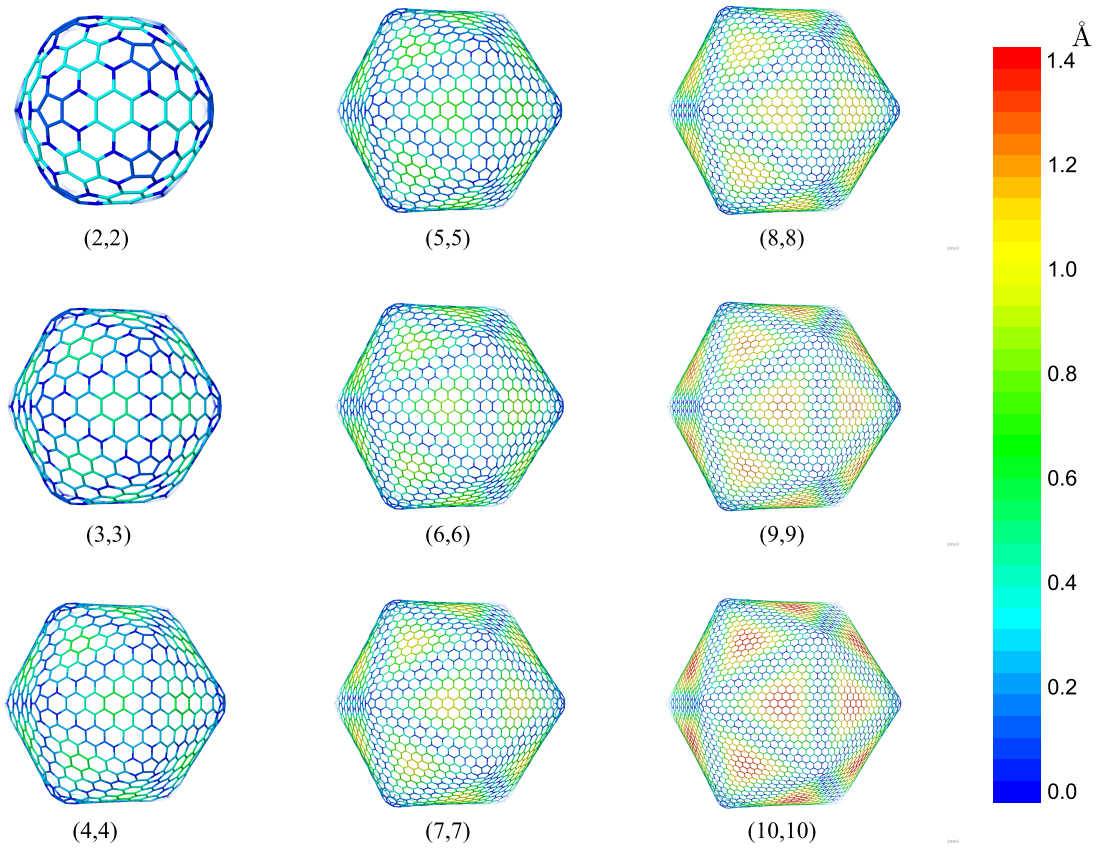

FIG. 5: Three-dimensional structures of (n, n) fullerenes ($n = 1$ not shown). For each face, atomic positions have been compared to the case of an ideally flat graphene triangle; relative displacements are rendered by means of a color scale (values in Å). The graphene triangle is taken so that its z coordinate corresponds to the radius of the inscribed sphere to the ideal polyhedral fullerene, and its central hexagon is in-plane aligned with the central hexagon of the fullerene face.

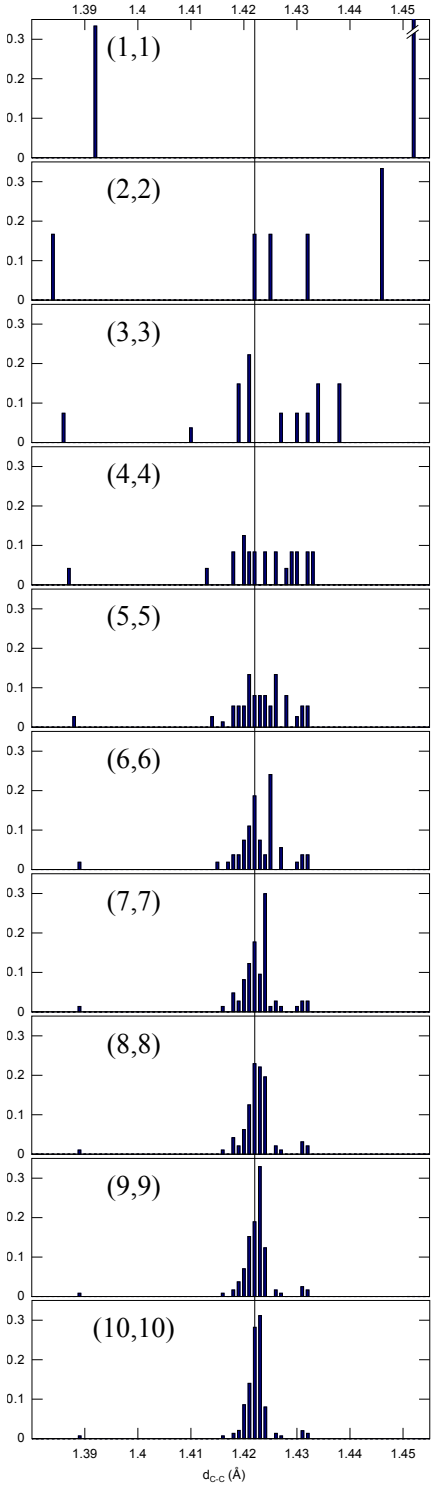

FIG. 6: Distribution of C-C bond lengths in (n, n) fullerenes. Lengths are in Å; populations of bonds are normalized, so that for each fullerene their total equals one. The narrow vertical line indicates the value for graphene (1.422 Å). In the case of (1,1), the population of bond length near 1.45 Å (not fully shown) is 0.667.

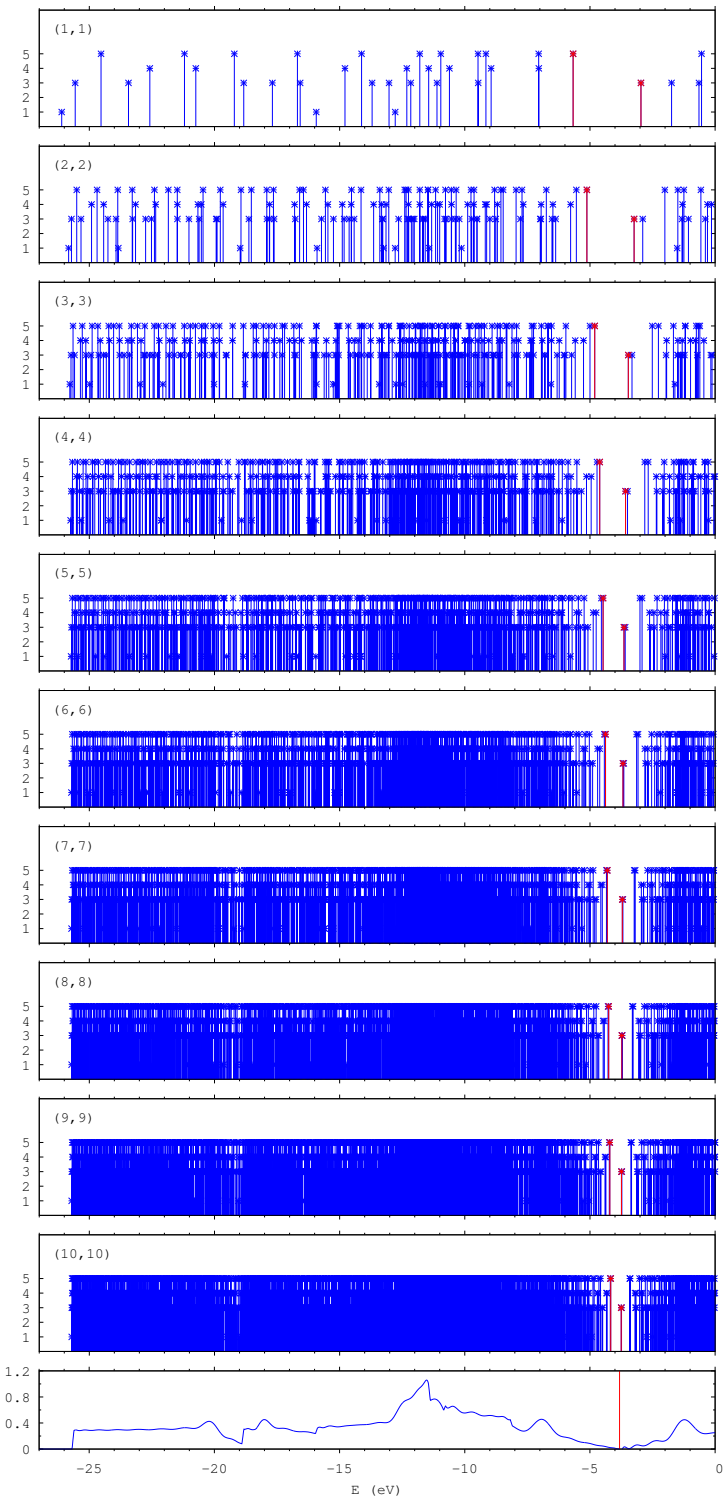

FIG. 7: Electronic levels of (n, n) fullerenes (along the x axis, in eV). For each level the corresponding degeneracy is reported along the y axis. HOMO and LUMO levels are in red. For sake of reference, density of states for graphene is shown in the bottom box (in states per eV per cell; Fermi level in red).

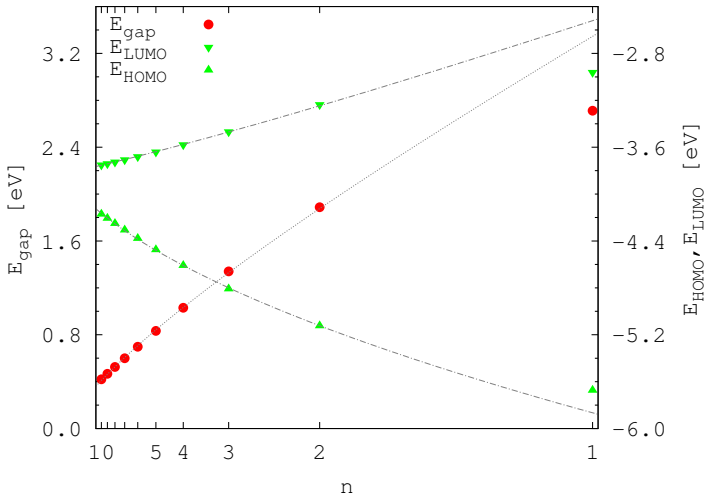

FIG. 8: Electronic band gap E_{gap} and HOMO and LUMO levels, E_{HOMO} and E_{LUMO}, of (n, n) fullerenes, all in eV, as a function of the n index. Points correspond to values obtained with the *ab initio* calculations. Curves are obtained through best-fit with respect to Eqs. (7), (8) and (9). Data for (1,1) are excluded from the fits (see text for details). The x axis is in inverse scale.

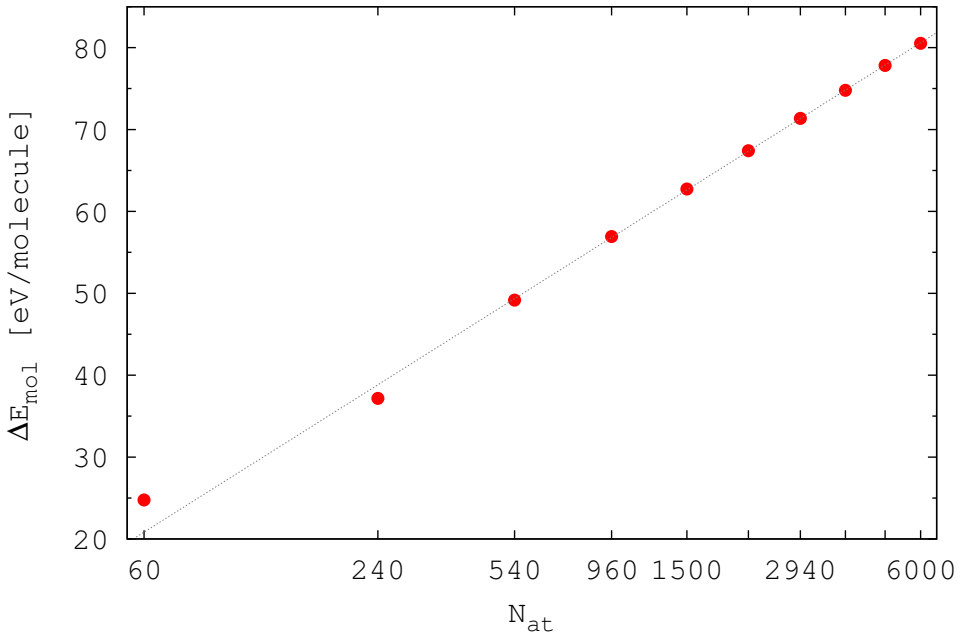

FIG. 9: Excess energy per molecule ΔE_{mol} of (n, n) fullerenes, in eV/molecule, as a function of the number of atoms N_{at}. Points correspond to values obtained with the *ab initio* calculations. The curve is obtained through best-fit with respect to Eq. (10). Data for (1,1) and (2,2) are excluded from the fit (see text for details). The x axis is in logarithmic scale.

(n,n)	(1,1)	(2,2)	(3,3)	(4,4)	(5,5)	(6,6)	(7,7)	(8,8)	(9,9)	(10,10)
n_{at}	1	3	6	10	15	21	28	36	45	55
N_{at}	60	240	540	960	1500	2160	2940	3840	4860	6000
N_{hex}	20	110	260	470	740	1070	1460	1910	2420	2990
N_{DOF}	2	7	15	26	40	57	77	100	126	155
N_{AO}	840	3360	7560	13440	21000	30240	41160	53760	68040	84000
ρ_{at}	60	80	90	96	100	102.8571	105	106.6667	108	109.0909

TABLE I: Parameters for (n,n) fullerenes with $n = 1 \div 10$. n_{at}, N_{at} and N_{hex} are the number of irreducible atoms, the number of atoms and the number of hexagons, respectively. N_{DOF} and N_{AO} are the number of internal degrees of freedom and the number of atomic orbitals, respectively. ρ_{at} is the ratio N_{at}/n_{at}.

(n,n)	(1,1)	(2,2)	(3,3)	(4,4)	(5,5)	(6,6)	(7,7)	(8,8)	(9,9)	(10,10)
$< r >$	3.544	7.070	10.548	14.027	17.511	21.002	24.491	27.983	31.475	34.968
r_{min}	3.544	6.940	10.215	13.528	16.864	20.217	23.562	26.912	30.260	33.608
r_{max}	3.544	7.332	11.342	15.378	19.420	23.464	27.512	31.560	35.610	39.660
Δr	0	0.392	1.127	1.850	2.556	3.247	3.950	4.648	5.350	6.052
ρ_r	1	1.056	1.110	1.137	1.152	1.161	1.168	1.173	1.177	1.180
E_{gap}	2.711	1.888	1.340	1.030	0.833	0.698	0.599	0.525	0.467	0.420
E_{HOMO}	-5.673	-5.124	-4.808	-4.609	-4.474	-4.378	-4.307	-4.251	-4.207	-4.171
E_{LUMO}	-2.962	-3.236	-3.468	-3.579	-3.641	-3.681	-3.707	-3.726	-3.740	-3.751
ΔE_{at}	412.71	154.83	91.04	59.31	41.82	31.21	24.27	19.48	16.01	13.42

TABLE II: Properties of (n,n) fullerenes with $n = 1 \div 10$. $< r >$ [Å] is the average radial distance over all atoms; r_{min} and r_{max} [Å] are the minimum and maximum radial distances, Δr [Å] and ρ_r are their difference and ratio, respectively. E_{gap} is the energy band gap [eV]. E_{HOMO} and E_{LUMO} are the energy levels [eV] of the Highest Occupied (HOMO) and Lowest Unoccupied (LUMO) Molecular Orbitals, respectively. ΔE_{at} is the excess energy per atom [meV/atom] with respect to the graphene sheet. The total energy of graphene is -1036.61114 eV/atom.

[1] H.W. Kroto, J.R. Heath, S.C. Obrien, R.F. Curl, and R.E. Smalley. C-60 - BUCKMINSTERFULLERENE. *Nature*, 318:162–163, 1985.

[2] F. Diederich and C. Thilgen. Covalent Fullerene Chemistry. *Science*, 271:317–323, 1996.

[3] D.S. Bethune, R.D. Johnson, J.R. Salem, M.S. de Vries, and C.S. Yannoni. Atoms in carbon cages: the structure and properties of endohedral fullerenes. *Nature*, 366:123–128, 1993.

[4] Y. Nishibayashi, M. Saito, S. Uemura, S. Takekuma, H. Takekuma, and Z. Yoshida. A non-metal system for nitrogen fixation. *Nature*, 428:279–280, 2004.

[5] M.R. Lee, R.D. Eckert, K. Forberich, G. Dennler, C.J. Brabec, and R. A. Gaudiana. Solar Power Wires Based on Organic Photovoltaic Materials. *Science*, 324:232–235, 2009.

[6] X. Gong, M. Tong, Y. Xia, W. Cai, J. Sun Moon, Y. Cao, G. Yu, C.-L. Shieh, B. Nilsson, and A.J. Heeger. High-Detectivity Polymer Photodetectors with Spectral Response from 300 nm to 1450 nm. *Science*, 325:1665–1667, 2009.

[7] J. Cami, J. Bernard-Salas, E. Peeters, and S.E. Malek. Detection of C60 and C70 in a Young Planetary Nebula. *Science*, 329:1180–1182, 2010.

[8] M. Chhowalla, H. Wang, N. Sano, K.B.K. Teo, S.B. Lee, and G.A.J. Amaratunga. Carbon Onions: Carriers of the 217.5 nm Interstellar Absorption Feature. *Phys. Rev. Lett.*, 90:155504, 2003.

[9] N.A. Marks, M. Lattemann, and D.R. McKenzie. Nonequilibrium Route to Nanodiamond with Astrophysical Implications. *Phys. Rev. Lett.*, 108:075503, 2012.

[10] S. Iijima. Direct Observation Of The Tetrahedral Bonding In Graphitized Carbon Black By High Resolution Electron Microscopy. *J. Cryst. Growth*, 50:675–683, 1980.

[11] D. Ugarte. Curling and closure of graphitic networks under electron-beam irradiation. *Nature*, 359:707–709, 1992.

[12] K.G. McKay, H.W. Kroto, and D.J. Wales. Simulated Transmission Electron Microscope Images and Characterisation of Concentric Shell and Icospiral Graphitic Microparticles. *J. Chem. Soc. Faraday Trans.*, 88:2815–2821, 1992.

[13] B.I. Dunlap, D.W. Brenner, J.W. Mintmire, R.C. Mowrey, and C.T. White. Local Density Functional Electronic Structures of Three Stable Icosahedral Fullerenes. *J. Phys. Chem.*, 95:8737–8741, 1991.

[14] D. York, J.P. Lu, and W. Yang. Density-functional calculations of the structure and stability of C240. *Phys. Rev. B*, 49:8526–8528, 1994.

[15] A.C. Tang, F.Q. Huang, Q.S. Li, and R.Z. Liu. Hückel treatment of carbon species with icosahedral symmetry. *Chem. Phys. Lett.*, 227:579–587, 1994.

[16] Y.-L. Lin and F. Nori. Electronic structure of single- and multiple-shell carbon fullerenes. *Phys. Rev. B*, 49:5020–5023, 1994.

[17] G.E. Scuseria. The equilibrium structures of giant fullerenes: faceted or spherical shape? An ab initio Hartree-Fock study of icosahedral C240 and C540. *Chem. Phys. Lett.*, 243:193–198, 1995.

[18] D. Bakowies, M. Bühl, and W. Thiel. Can Large Fullerenes Be Spherical? *J. Am. Chem. Soc.*, 117:10113–10118, 1995.

[19] C.H. Xu and G.E. Scuseria. An O(N) tight-binding study of carbon clusters up to C8640: the geometrical shape of the giant icosahedral fullerenes. *Chem. Phys. Lett.*, 262:219–226, 1996.

[20] B.I. Dunlap and R.R. Zope. Efficient quantum-chemical geometry optimization and the structure of large icosahedral fullerenes. *Chem. Phys. Lett.*, 422:451–454, 2006.

[21] P. Calaminici, G. Geudtner, and A.M. Köster. First-Principle Calculations of Large Fullerenes. *J. Chem. Theory Comput.*, 5:29–32, 2009.

[22] R. Dovesi, V. R. Saunders, C. Roetti, R. Orlando, C. M. Zicovich-Wilson, F. Pascale, B. Civalleri, K. Doll, N. M. Harrison, I. J. Bush, Ph. D'Arco, M. Llunell, M. Causà, and Y. Noël. *CRYSTAL14 User's Manual*. Università di Torino, Torino, 2014.

[23] R. Dovesi, R. Orlando, A. Erba, C.M. Zicovich-Wilson, B. Civalleri, S. Casassa, L. Maschio, M. Ferrabone, M. De La Pierre, Ph. D'Arco, Y. Noël, M. Causà, M. Rérat, and B. Kirtman. CRYSTAL14: A Program for the Ab Initio Investigation of Crystalline Solids. *Int. J. Quantum Chem.*, page DOI:10.1002/qua.24658, 2014.

[24] P. Schwerdtfeger, L. Wirz, and J. Avery. Program Fullerene a Software Package for Constructing and Analyzing Structures of Regular Fullerenes. *J. Comput. Chem.*, 34:1508–1526, 2013.

[25] G. Brinkmann, O.D. Friedrichs, S. Lisken, A. Peeters, and N. Van Cleemput. CaGe a Virtual Environment for Studying Some Special Classes of Plane Graphs an Update. *MATCH Commun. Math. Comput. Chem.*, 63:533–552, 2010.

[26] TURBOMOLE V6.5 2013, a development of University of Karlsruhe and Forschungszentrum Karlsruhe GmbH, 1989-2007, TURBOMOLE GmbH, since 2007; available from

`http://www.turbomole.com`.

[27] A. D. Becke. Density functional theochemistry. III The role of exact exchange. *J. Chem. Phys.*, 98:5648–5652, 1993.

[28] C. Lee, W. Yang, and R. G. Parr. Development of the Colle-Salvetti correlation-energy formula into a functional of the electron density. *Phys. Rev. B*, 37:785–789, 1988.

[29] P. J. Stephens, F. J. Devlin, C. F. Chabalowski, and M. J. Frisch. *Ab initio* calculation of vibrational absorption and circular dichroism spectra using density functional force fields. *J. Phys. Chem.*, 98:11623–11627, 1994.

[30] C. M. Zicovich-Wilson, Y. Noël, A. M. Ferrari, R. Orlando, M. De La Pierre, and R. Dovesi. On the use of symmetry in SCF calculations. The case of fullerenes and nanotubes. *AIP Conf. Proc.*, 1456:248–255, 2012.

[31] R. Orlando, M. De La Pierre, C. M. Zicovich-Wilson, A. Erba, and R. Dovesi. On the full exploitation of symmetry in periodic (as well as molecular) SCF *ab initio* calculations. *submitted to J. Chem. Phys.*, 2014.

[32] M. De La Pierre, R. Orlando, M. Ferrabone, C. M. Zicovich-Wilson, and R. Dovesi. Exploitation of symmetry in periodic SCF *ab initio* calculations: application to large 3D compounds. *submitted to Sci. China Chem.*, 2014.

[33] Y. Noël, Ph. D'Arco, R. Demichelis, C.M. Zicovich-Wilson, and R. Dovesi. On the Use of Symmetry in the Ab Initio Quantum Mechanical Simulation of Nanotubes and Related Materials. *J. Comput. Chem.*, 31:855–862, 2010.

[34] R. Demichelis, Y. Noël, Ph. D'Arco, M. Rérat, C.M. Zicovich-Wilson, and R. Dovesi. Properties of Carbon Nanotubes: An ab Initio Study Using Large Gaussian Basis Sets and Various DFT Functionals. *J. Phys. Chem. C*, 115:8876–8885, 2011.

[35] R. Orlando, R. Bast, K. Ruud, U. Ekström, M. Ferrabone, B. Kirtman, and R. Dovesi. The First and Second Static Electronic Hyperpolarizabilities of Zigzag Boron Nitride Nanotubes. An ab Initio Approach through the Coupled Perturbed Kohn-Sham Scheme. *J. Phys. Chem. A*, 115:12631–12637, 2011.

[36] M. Ferrabone, B. Kirtman, M. Rérat, R. Orlando, and R. Dovesi. Polarizability and hyperpolarizability of BN zigzag nanotubes calculated by the coupled perturbed Kohn-Sham scheme. *Phys. Rev. B*, 83:235421, 2011.

[37] M. Ferrabone, B. Kirtman, V. Lacivita, M. Rérat, R. Orlando, and R. Dovesi. Vibrational

Contribution to Static and Dynamic (Hyper)Polarizabilities of Zigzag BN Nanotubes Calculated by the Finite Field Nuclear Relaxation Method. *Int. J. Quantum Chem.*, 112:2160–2170, 2012.

[38] M. De La Pierre, P. Karamanis, J. Baima, R. Orlando, C. Pouchan, and R. Dovesi. Ab Initio Periodic Simulation of the Spectroscopic and Optical Properties of Novel Porous Graphene Phases. *J. Phys. Chem. C*, 117:2222–2229, 2013.

[39] L. Ge, B. Montanari, J.H. Jefferson, D.G. Pettifor, N.M. Harrison, and G.A.D. Briggs. Modeling spin interactions in carbon peapods using a hybrid density functional theory. *Phys. Rev. B*, 77:235416, 2008.

[40] V. Lacivita, M. Rérat, R. Orlando, M. Ferrero, and R. Dovesi. Calculation of longitudinal polarizability and second hyperpolarizability of polyacetylene with the coupled perturbed Hartree-Fock/Kohn-Sham scheme: where it is shown how finite oligomer chains tend to the infinite periodic polymer. *J. Chem. Phys.*, 136:114101, 2012.

[41] V. Lacivita, M. Rérat, B. Kirtman, R. Orlando, M. Ferrabone, and R. Dovesi. Static and dynamic coupled perturbed Hartree-Fock vibrational (hyper)polarizabilities of polyacetylene calculated by the finite field nuclear relaxation method. *J. Chem. Phys.*, 137:014103, 2012.

[42] K. Doll. Implementation of analytical Hartree-Fock gradients for periodic systems. *Comput. Phys. Comm.*, 137:74–88, 2001.

[43] K. Doll, V. R. Saunders, and N. M. Harrison. Analytical Hartree-Fock gradients for periodic systems. *Int. J. Quantum Chem.*, 82:1–13, 2001.

[44] B. Civalleri, P. D'Arco, R. Orlando, V. R. Saunders, and R. Dovesi. Hartree-Fock geometry optimization of periodic system with the CRYSTAL code. *Chem. Phys. Lett.*, 348:131–138, 2001.

[45] C. G. Broyden. The Convergence of a Class of Double-rank Minimization Algorithms 1. General Considerations. *J. Inst. Math. Appl.*, 6:76–90, 1970.

[46] R. Fletcher. A new approach to variable metric algorithms. *Comput. J.*, 13:317–322, 1970.

[47] D. Goldfarb. A Family of Variable-Metric Methods Derived by Variational Means. *Math. Comput.*, 24:23–26, 1970.

[48] D. F. Shanno. Conditioning of quasi-Newton methods for function minimization. *Math. Comput.*, 24:647–656, 1970.

[49] Jmol 3d engine.
`http://jmol.sourceforge.net`.

[50] Jmoledit applet.

http://www.theochem.unito.it/crystal_tuto/mssc2008_cd/tutorials/webvib/index.html.

[51] Inkscape program.

http://www.inkscape.org.

[52] Libreoffice suite.

http://www.libreoffice.org.

[53] Octave environment.

http://www.gnu.org/software/octave.

[54] Gnuplot utility.

http://www.gnuplot.info.

[55] H.S. Seung and D.R. Nelson. Defects in flexible membranes with crystalline order. *Phys. Rev. A*, 38:1005–1018, 1988.

[56] J. Tersoff. Energies of fullerenes. *Phys. Rev. B*, 46:15546–15549, 1992.

[57] A. Siber. Energies of sp^2 carbon shapes with pentagonal disclinations and elasticity theory. *Nanotechnol.*, 17:3598–3606, 2006.

[58] G.G. Tibbetts. Why are carbon filaments tubular. *J. Cryst. Growth*, 66:632–638, 1984.

[59] D.H. Robertson, D.W. Brenner, and J.W. Mintmire. Energetics of nanoscale graphitic tubules. *Phys. Rev. B*, 45:12592–12595, 1992.

[60] J. Kürti, G. Kresse, and H. Kuzmany. First-principles calculations of the radial breathing mode of single-wall carbon nanotubes. *Phys. Rev. B*, 58:8869–8872, 1998.

[61] K.N. Kudin, G.E. Scuseria, and B.I. Yakobson. C_2F, BN and C nanoshell elasticity from ab initio computations. *Phys. Rev. B*, 64:235406, 2001.

[62] D. Sánchez-Portal, E. Artacho, J.M. Soler, A. Rubio, and P. Ordejón. Ab initio structural, elastic, and vibrational properties of carbon nanotubes. *Phys. Rev. B*, 59:12678–12688, 1999.

[63] R.C. Haddon, G.E. Scuseria, and R.E. Smalley. C_{240} - The most chemically inert fullerene? *Chem. Phys. Lett.*, 272:38–42, 1997.